Self-Assembly of Inorganic Nanocrystals: Fabrication and Collective Intrinsic Properties

M.-P. PILENI*

Laboratoire LM2N, Université Pierre et Marie Curie (Paris VI), BP 52, 4 Place Jussieu, F-75231 Paris Cedex 05, France

Received February 12, 2007

ABSTRACT

In this Account, we demonstrate that the ordering of nanocrystals over long distances in 3D superlattices, called supracrystals, can lead to unexpected results: the emergence of collective intrinsic properties. The shape of the nanocrystal organization at the mesoscopic scale also induces new physical properties. In addition, we show that nanocrystals can be used as masks for lithography.

Introduction

Self-organization of entities in 2D and 3D is one of the basic processes in nature. Spherical objects, such as oranges, balls, or particles, having the same diameter self-organize in compact hexagonal networks (2D) and in 3D-ordered structures [face-centered cubic (fcc) or hexagonal close packed (hcp)]. For example, opals made of silica particles having a few micrometers diameter self-organize in a highly ordered structure,[1] such as atoms in the bulk phase or sodium and chloride ions in NaCl. Similarly, biological systems consist of self-assemblies of organic molecules with either covalent or hydrogen bonding. In some cases, nature combines the biochemical system and inorganic materials to produce various types of materials. One of the most well-known systems is the magnetotactic bacteria,[2] where it is sometimes found that these organizations possess specific physical properties as a result of the ordering. As an example, the change in the opal color is due to diffraction effects from arrays of uniformly sized spheres of amorphous silica (170–359 nm in diameter). The spacing of the regular optical discontinuities in the arrays is determined by the diameter of the spheres, and this in turn determines the maximum wavelength that can be diffracted, similar to the diffraction of X-rays of atoms in a crystal.[1] The magnetotactic bacteria are sensitive to the magnetic field of the earth because Fe_30_4 micrometer particles surrounded by lipids, called magnetosomes, are aligned inside the bacteria.[2] Many other examples exist in nature.

A large community has developed the concept observed with natural opals to artificial crystalline solids formed from several micrometer building blocks usually called photonic crystals that are approximately 1000 times larger than the atoms in traditional molecular crystals.[3] Other methods developed to fabricate and impose patterns on nanostructures at the micrometer scale[4] produce fascinating phenomena.

At the nanometric scale, the particles are almost smaller by 1 or 2 orders of magnitude compared to the building blocks described above. The first self-assembly of particles having a diameter of a few nanometers (<10 nm) was discovered 10 years ago.[5,6] Later, several groups demonstrated that a rather large number of nanocrystals were locally ordered.[5–14] The 3D superlattices were made of a few nanocrystal layers.[11,15,16] To be able to find new physical properties as a result of the ordering, the nanocrystals have to be ordered at the mesoscopic scale. Relatively very few groups have been able to produce 3D superlattices made of several thousand layers, called supracrystals. These were obtained for silver,[17–19] CdSe,[6,20] cobalt,[21,22] and gold[23] nanocrystals.

The collective physical properties of an assembly of nanocrystals[7,8] are neither those of the isolated particles nor those of the corresponding bulk phase. They may depend upon the shape and the nanocrystal assembly at the mesoscopic scale. Collective optical[24] and magnetic[25,26] properties because of dipolar interactions are observed when the nanocrystals are organized in 2D superlattices.[7,8] The optical properties of 5 nm silver nanocrystals organized in hexagonal networks give rise to several plasmon resonance modes, which are attributed to the film anisotropy. In the magnetic properties, the hysteresis loop of nanocrystals is squarer when they are deposited in compact hexagonal networks compared to isolated nanocrystals. The calculated and experimental hysteresis loops for a chain-like structure are squarer than that of a well-ordered array of nanocrystals. The linear chains of nanocrystals behave as homogeneous nanowires.

Here, we demonstrate that the ordering of nanocrystals at the mesoscopic scale, in 3D supracrystals, is not simply an esthetic arrangement but is in fact a new generation of materials. We first show the various types of nanocrystal self-assemblies and designate the parameters needed to produce them at the mesoscopic scale. Then, we describe the various intrinsic mechanical, optical, magnetic, and crystal-growth collective intrinsic properties as a result of

Marie-Paule Pileni is a Distinguished Professor and Director of the Mesoscopic and Nanometric Materials Laboratory at the Université Pierre et Marie Curie and chair of Institut Universitaire de France. She studied the development of structure–reactivity relationships in organized molecular systems and, with regard to the physical properties of these new materials, developed the self-organization of the nanocrystals in compact hexagonal networks (2D) and face-centered cubic structures (3D) at the mesoscopic scale. In 1999, she demonstrated the specific collective properties of these assemblies. In addition, she proved the existence of collective intrinsic properties (optical, mechanical, and crystal growth) to these assemblies. Between 1999 and 2006, she received the Langmuir award of the American Chemical Society, the lecture award of the Japanese Chemical Society, the Research Award of the Alexander von Humboldt Foundation in Germany, the Descartes–Huygens Prize of the Royal Netherlands Academy of Arts and Science, and the Emilia Valeri award from the French Academy of Science. In addition, she was the French citation laureate and was awarded the Institute of Scientific Information Award for most quoted French scientist between 1981 and 1998. She is a member of of the Royal Swedish Academy of Engineering Sciences, chair of a scientific committee of the engineering and material sciences division of the European Academy of Science, and has a doctorate honoris causa from Chalmers University, Göteborg, Sweden. She is a Chevalier dans l'Ordre National de la Légion d'Honneur and Officier dans l'Ordre National du Mérite.

* To whom correspondence should be addressed. E-mail: pileni@sri.jussieu.fr.

10.1021/ar6000582 CCC: $37.00
Published on Web 05/02/2007

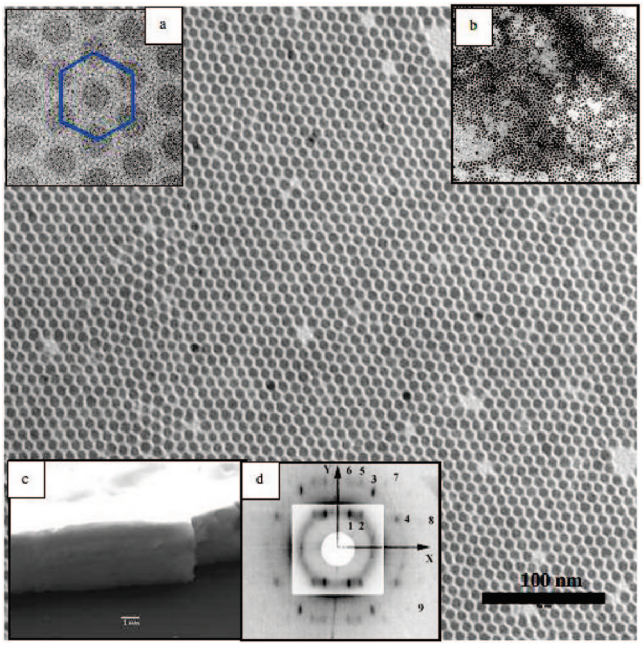

FIGURE 1. Monolayer of 7 nm cobalt nanocrystals over a very long distance. (Inset a) Transmission electron microscopy (TEM) pattern showing that the nanocrystals are organized in a hexagonal network. (Inset b) TEM pattern shows no organization in 2D when the nanocrystals do not have similar sizes. (Inset c) Scanning electron microscopy (SEM) pattern of the pavement of 7 nm cobalt nanocrystals, called supracrystals. (Inset d) X-ray diffraction pattern showing a pure fcc structure.

the nanocrystal ordering. We show that the shape of the mesostructure made with nanocrystals controls the physical properties of 3D superlattices. Finally, we demonstrate that nanocrystals can be used as masks for lithography.

Self-Organization of Inorganic Nanocrystals

1. How to Order Nanocrystals? The nanocrystals described below are made in water-in-oil droplets stabilized by a surfactant and called reverse micelles.[27] At the end of the synthesis, the nanocrystals are coated with surfactants that may have different polar head groups.[7] For silver nanocrystals, the most often used surfactant is dodecanethiol, and for cobalt and iron oxide nanocrystals, the most often used surfactant is dodecanoic acid. All of the experiments described below are done with these two surfactants unless otherwise stated. The polar head group of the coating surfactant remains the same; only the chain length and solvent differ. After washing, the coated nanocrystals are dispersed in a given solvent. By deposition of such a solution on a substrate, the nanocrystals are ordered in compact hexagonal networks if their size distribution is low enough (inset b in Figure 1).[7] Of course, because of van der Waals interactions, the ordering is easier for larger nanocrystals. When the size distribution is rather large (up to 13%), no compact packing can be obtained (inset d in Figure 1). Hence, the size distribution is the key parameter in producing compact nanocrystal ordering. However, it is not the only one. Particle–particle and particle–substrate interactions[28] play an important role in this ordering. Hence, the ordering is better with

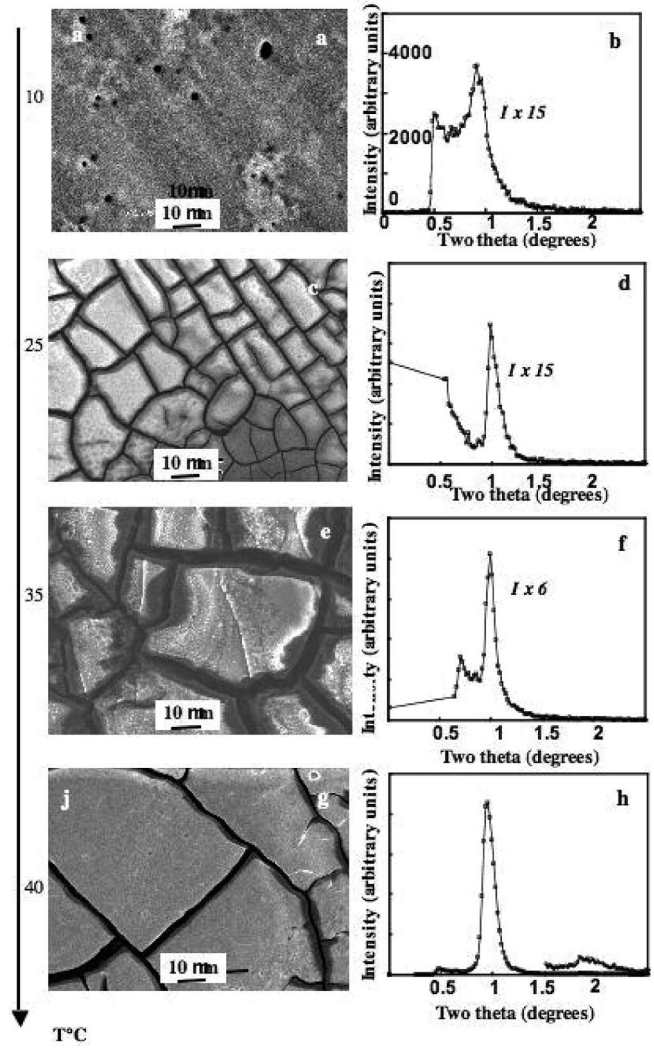

FIGURE 2. SEM patterns and X-ray diffraction patterns obtained by the deposition of cobalt nanocrystals on the HOPG substrate at various temperatures. The different substrate temperatures, T, and corresponding X-ray diffraction patterns are $T = 10$ °C (a and b), $T = 25$ °C (c and d), $T = 35$ °C (e and f), and $T = 45$ °C (g and h).

silver and cobalt nanocrystals on HOPG (Highly Oriented Pyrolitic Graphite) than amorphous carbon[19,20] whereas the opposite is the case for Ag_2S.[5]

Other structures of nanocrystals, such as rings, fingers, etc., are governed by Marangoni instabilities[7] and mainly depend upon the temperature gradient induced during the solvent evaporation process and not the parameters described above.

2. Tune the Nanocrystals Ordering. When cobalt (or silver) nanocrystals are able to self-organize in compact hexagonal networks over long distances (Figure 1), a regular periodic arrangement of nanocrystals in 3D superlattices, called supracrystals,[17–19,21,22] with more than 1000 layers of organized nanocrystals occurs (inset c in Figure 1). The X-ray diffraction spots of a fcc-ordered structure are formed (inset d in Figure 1). To determine the influence of the nanocrystal ordering on the physical properties of such assemblies, we need to produce simultaneously, with the same batch of nanocrystals, both supracrystals and disordered aggregates. This is possible

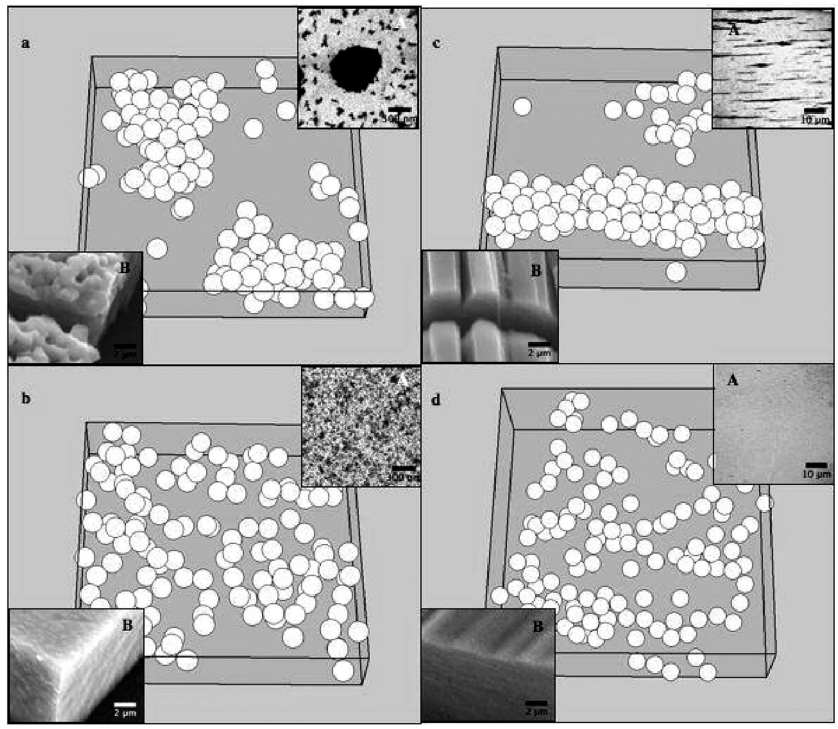

FIGURE 3. Snapshots of the configurations by the Brownian dynamics simulations. For the coating layer thickness, $d = 1.2$ nm (a and c) and $d = 1.6$ nm (b and d) without (a and b) or with (c and d) an applied field. (Inset A) TEM patterns obtained with C8 (a and c) and C12 (b and d) without (a and b) or with (c and d) an applied field. (Inset B) SEM patterns obtained with C8 (a and c) and C12 (b and d) without (a and b) or with (c and d) an applied field.

by changing the substrate temperature during the deposition of nanocrystals on the substrate. At low temperatures, the deposition gives rise to the formation of a nonhomogeneous thin film coexisting with aggregates (Figure 2a). The X-ray diffraction pattern (Figure 2b) has a broad diffuse ring attributed to a disordered material. Upon increasing the substrate temperature ($10 < T < 45$ °C), the film morphology and the pavement area changes (parts c, e, and g of Figure 2). Simultaneously, the X-ray diffraction intensity increases (parts d, f, and h of Figure 2) with the appearance of a second-order diffraction. This clearly shows an increase in the nanocrystal-ordering degree with a fcc structure. Thus, it is possible to tune the nanocrystal ordering from disordered aggregates to supracrystals. From these results, it is claimed that, even if the same forces are not involved, nanocrystals are able to behave as atoms with the formation of either amorphous or crystalline materials as for example, amorphous carbon or diamond.

3. Control the Shape of the Nanocrystal Assemblies. Let us consider nanocrystals having a low dipole interaction with respect to the thermal energy and differing by the average distances between them (interdistance) from 1.2 to 1.6 nm. Dynamic Brownian simulation taking into account the interparticle interaction, defined as a sum of the steric repulsion, the dipole–dipole potential, and the van der Waals attraction, shows the formation, during the evaporation process, of large spherical aggregates (Figure 3a) when the distance between particles is 1.2 nm, whereas they are randomly dispersed (Figure 3b) for an interdistance of 1.6 nm. Similarly, when a magnetic field is applied during the evaporation process, the thick-striped structures in the direction of the applied field (Figure 3c) are observed for an interdistance of 1.2 nm, whereas a random nanocrystal organization (Figure 3d) is produced for a 1.6 nm nanocrystal interdistance. These patterns are explained as follows: when the distances between particles are small enough, aggregates are formed because of the van der Waals forces, enhancing considerably the long-range dipolar forces compared to isolated particles. This is accompanied by the formation of a "macro-dipolar moment" leading to an anisotropic organization of the nanoparticles (Figure 3c). Upon increasing the interparticle distance, the van der Waals interactions are too weak to form aggregates and particles behave individually. No aggregation of the particles is observed even when particles are subjected (Figure 3d) or not subjected (Figure 3c) to an applied magnetic field during the evaporation. To improve this model, 10 nm γ-Fe_2O_3 nanocrystals are coated by surfactants with different alkyl chain lengths dispersed in cyclohexane. During the evaporation process, a magnetic field is applied or not applied. At the end of evaporation, SEM patterns show the following behavior: With C8, large aggregates are observed with no field (inset A in Figure 3a), whereas the nanocrystals are aligned in an applied one (inset A in Figure 3c). With C12, the nanocrystals are dispersed on the substrate with (inset A in Figure 3d) and without (inset A in Figure 3b) an applied field. Such behavior is reinforced upon increasing the nanocrystal concentration with the appearance of rough-surface nanocrystals coated with C8 (inset

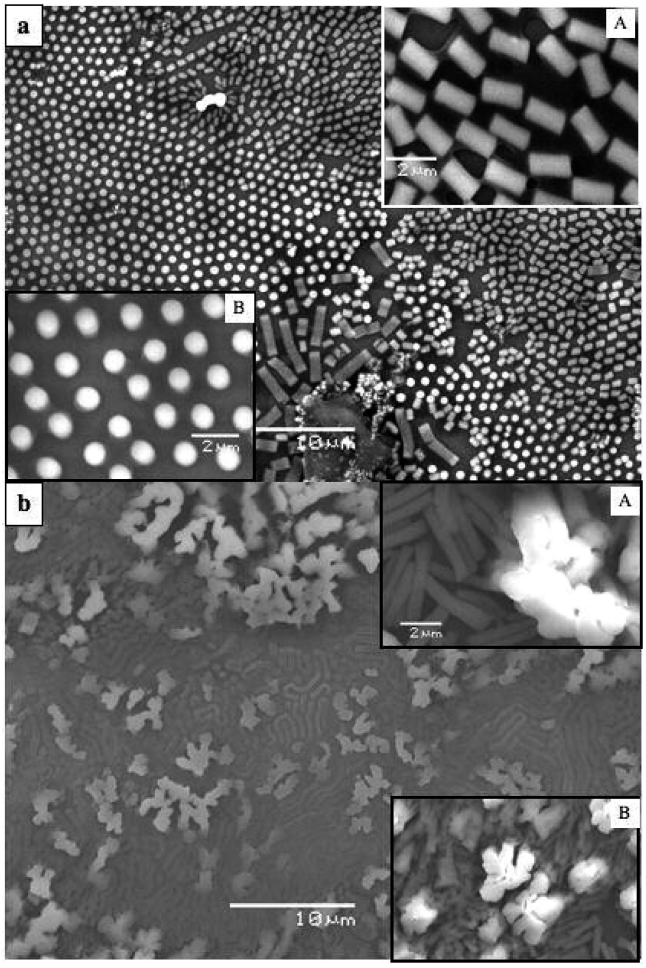

FIGURE 4. SEM patterns of mesostructures of 5.7 nm cobalt nanocrystals having 13% (a) and 18% (b) size distributions.

B in Figure 3a) and wires (inset B in Figure 3c), whereas with C12, a thin film is formed (insets B in parts b and d of Figure 3) in the absence and presence of an applied magnetic field, respectively. Hence, from the same nanocrystals, it is possible to produce either a homogeneous film or nanocrystal wires.[29] This makes it possible to determine whether or not the shape of the mesocopic structure changes the magnetic properties of the assemblies.

Intrinsic Properties of Long-Distance Ordering of Nanocrystals in Either Supracrystals or Multilayers

1. Mechanical Intrinsic Properties. When a magnetic field perpendicular to the substrate is applied during the evaporation of 5.7 nm cobalt nanocrystals dispersed in hexane and characterized by a very low size distribution (13%),[30–32] mainly dots (upright or fallen columns) are produced at the end of the evaporation (Figure 4a). Conversely, when the size distribution increases (18%), keeping a similar average diameter (5.9 nm), a large number of flower-like structures as a result of coalescence of either upright or fallen columns forming worm-like and labyrinthine shapes are produced (Figure 4b). The proposed mechanism of pattern formation is the following: during the evaporation process, a liquid–gas phase transition[31,32] occurs with the formation of a concentrated solution of nanocrystals in equilibrium with a diluted one. In the concentrated phase, columns (dots) are progressively formed and tend to migrate to self-organize in hexagonal patterns. When the size distribution is low enough, the nanocrystals dispersed in solution tend to self-assemble in fcc supracrystals with the formation of well-defined and compact columns, whereas at higher size distribution values, the interactions between particles markedly decrease and the columns are formed with disordered entities. This creates defects. The cohesive forces between columns are not large enough to keep them ordered, and columns tend to fuse to form labyrinths. Hence, the mesoscopic structure of cobalt nanocrystals is tuned from well-defined dots to labyrinths with an increasing nanocrystal size distribution from 13 to 18% while keeping the same average nanocrystal size. The mechanical properties of the column formation control the final patterns.

2. Vibrational Collective Coherence Properties. Silver nanoparticles markedly absorb light by the excitation of electronic surface plasma dipolar oscillations.[33] This resonance induces intense Raman scattering by the vibration of the nanoparticles. The low-frequency Raman spectra of these materials always show a very intense peak close to the Rayleigh line, which is attributed to the excitation of the quadrupolar vibration mode of the nanoparticles via the plasmon–phonon interaction.

For disordered aggregates of silver nanocrystals (solid line), the quadrupolar modes appear as sharp intense lines (Figure 5a). For spherical nanocrystals with sizes larger than ~1 nm, the cluster vibrations are described by modeling the nanocrystal with a continuum nanosphere of a diameter D equal to the size of the nanocrystal[34] and using the longitudinal, v_l, and transversal, v_t, sound velocities of bulk Ag. The frequencies are given by the following equation:

$$\nu = \frac{S_{ln} v_t}{D} \tag{1}$$

where S_{ln} depends upon the ratio v_l/v_t. Figure 5b shows that the line shape agrees with the inverse-size histogram because the intensity of the Raman scattering frequency is inversely proportional to the nanocrystal diameter. As already discovered,[35] this indicates that there is *intra*-nanoparticle coherence, i.e., nanocrystallinity, and not *inter*-nanocrystal coherence.

When the supracrystals are smaller than $^1/_{10}$ of the excitation wavelength, the Raman peak corresponding to quadrupolar modes is shifted toward a lower frequency compared to the disordered aggregate Raman peak (Figure 5a), with a decrease in its width (Figure 5c). This change is due to two effects:

(i) *Effect of the Lorentz field.* The electromagnetic field, induced on each nanocrystal by the vibration-fluctuating electric dipoles of the neighboring nanocrystals organized in fcc supracrystals, changes the nanocrystal polarizability fluctuation.

(ii) *Effect of vibrational coherence.* The van der Waals bonding between thiol chains is sufficient to establish a

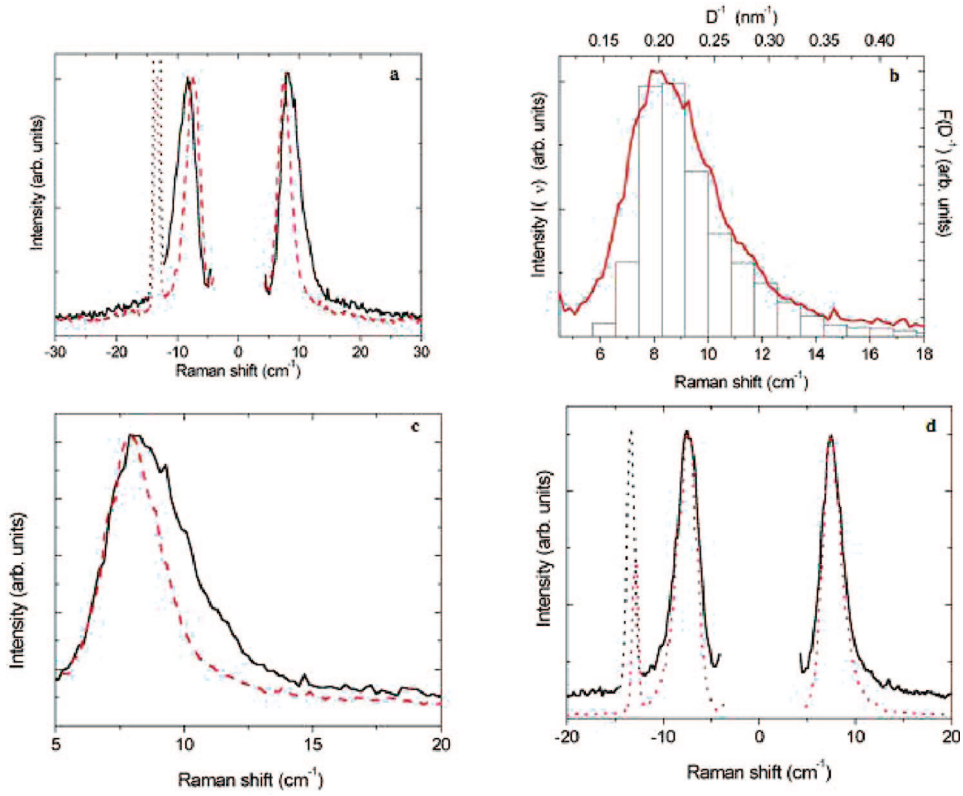

FIGURE 5. (a) Raman scattering spectra of 5 nm silver nanocrystals forming either disordered aggregates (black) or a supracrystal (red). (b) Comparison of the Stokes line shapes of disordered aggregates. (c) Superposition of Stokes line shapes after horizontal shifting of disordered aggregates and the supracrystal. (d) Comparison of the Raman scattered intensity $I^s(\nu)$ from silver nanocrystals forming small supracrystals with the profile $[I^\delta(\nu)]^2$ from disordered aggregates of silver nanocrystals.

correlation between the vibrating nanocrystals, so that they vibrate coherently in a supracrystal. The light is scattered by stationary modes in the supracrystal, as by the vibration modes in a molecule. The active vibration modes are regarded as localized, and they are determined only by their symmetry. The intensity of Raman scattering from a supracrystal, $I^s(\nu)$,[36] is

$$I^s(\nu) = L^2(\nu)[I^\delta(\nu)]^2 \qquad (2)$$

where ν, $I^\delta(\nu)$, and $L(\nu)$ are the frequency, the Raman scattering intensity for disordered aggregates, and the Lorentz field factor, respectively. The Stokes and anti-Stokes $I^s(\nu)$ profiles are horizontally shifted and vertically rescaled to match the peak maxima. The line profile is given by the square of that corresponding to nanocrystal disordered arrangements. The narrowed peak of the "small" supracrystals has the same profile as the square of the non-narrowed peak of the "disordered" aggregates (Figure 5d). These data clearly indicate inter-nanocrystal coherence inside fcc supracrystals.[19] Hence, again, although the forces involved are not the same, nanocrystals in a supracrystal behave as atoms in a nanocrystal. These data are confirmed by using a femtosecond reflectivity dynamics with collective vibration of cobalt nanocrystals in a supracrystal.[37] These coherences could explain the change in the transport properties observed previously with silver nanocrystal self-organizations.[38]

3. Magnetic Intrinsic Collective Properties. A general feature characterizing single magnetic nanocrystals is their superparamagnetic behavior. The magnetocrystalline anisotropy energy in axial symmetry depends mainly upon the particle volume, V, and its anisotropy constant, K. In the superparamagnetic regime, the anisotropy energy barrier, $E_b = KV$, is usually of the same magnitude as the thermal energy. Then, the magnetization vector fluctuates among the easy directions of magnetization. This process is called superparamagnetic relaxation. When a magnetic material is subjected to an increasing magnetic field, the spins within the material are aligned with the field. Its magnetization increases and reaches a maximum value called the saturation magnetization, M_s. As the magnitude of the magnetic field decreases, spins cease to be aligned with the field to reach the remanance, M_r, at zero applied field. The spins become totally disordered at the coercivity field, H_c. If the magnetic sample is cooled to a low temperature (3 K) and then a magnetic field is applied (20 Oe), a progressive increase in the magnetization is observed to reach a maximum called the blocking temperature, T_B). At higher T_B values, the magnetization of the particle does not depend upon the temperature and the susceptibility falls. This is called zero-field-cooled (ZFC) magnetization.

Figure 6a shows the ZFC curve normalized to the blocking temperature (T_B) versus the temperature curves of both the ordered (red) and disordered (black) supracrystals of 7 nm cobalt assemblies.[39,40] The ZFC peak is significantly narrower for the ordered sample. The width of the ZFC peak is related to the distribution of energy barriers, E_b, in the system: a larger distribution gives a broader peak. The energy barriers involved are the ani-

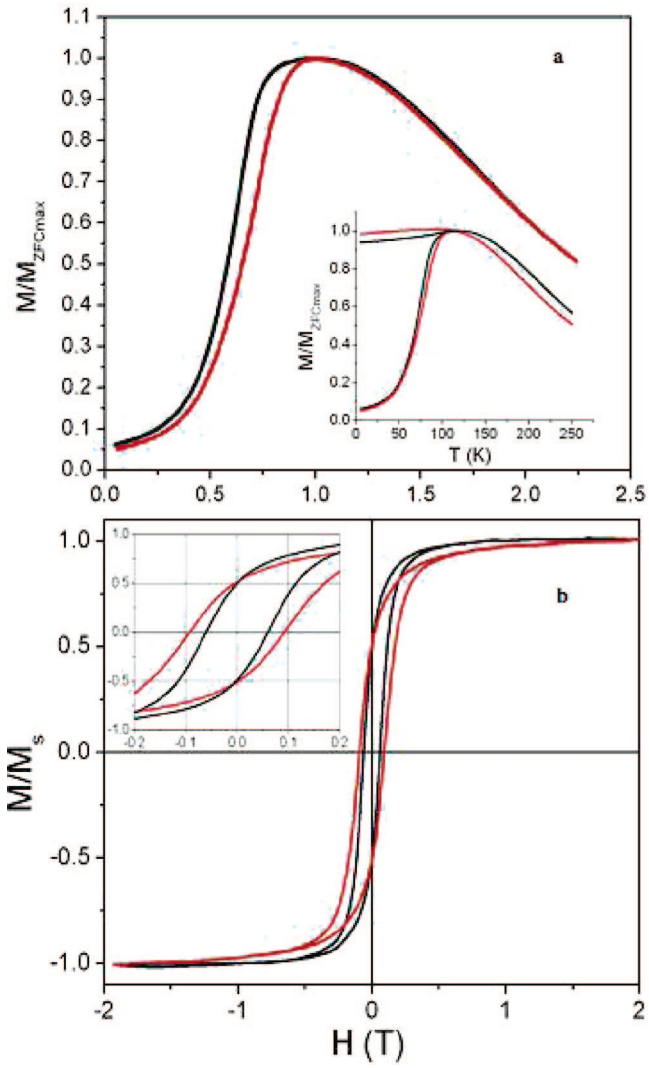

FIGURE 6. (a) Normalized to the blocking temperature, the ZFC curve of amorphous aggregates (red) and supracrystals (black), corresponding to these configurations calculated for 8 nm cobalt nanocrystals and 0.125 as an effective coupling constant. (b) *M* versus *H* curves of disordered (black line) and ordered (red line) 3D assemblies. (Inset) Enlargement of the low-field region.

sotropy energy ($E_a = k_a V$, where k_a is the anisotropy constant and V is the nanoparticle volume) and the dipole–dipole interaction energy (E_{dd}), which varies with the particle distance.[41] Because the ordered and disordered samples are made with the same batch of nanocrystals, this change in width of the ZFC peak is not a consequence of a change in the size dispersion of nanoparticles between the two samples or a difference in anisotropy. We therefore explain the difference in the distribution of E_b by the change in the structural environment of the Co nanoparticles. As pointed out, dipolar forces have a strong directional dependence, and consequently, dipolar interactions in the assembly should be sensitive to the detailed geometrical arrangement of the nanoparticles. In the supracrystals, the fcc domains have long coherence lengths and therefore the geometric environment of the nanoparticles is fairly uniform. In the disordered 3D aggregates, we have a mixture of many very small fcc domains characterized by a short coherence length and disordered domains with an irregular stacking periodicity. Therefore, we expect the distribution of E_{dd} (and hence E_b) in the supracrystal sample to be lower than in the disordered sample, leading to the observed narrowing of the ZFC peak. We acknowledge that this effect of order is fairly subtle; however, we have found that it is highly reproducible. Figure 6b shows the magnetization versus field curves for the ordered and disordered samples at 5 K. In both cases, saturation is reached at around 1 T and hysteresis is observed. For the ordered sample, H_c is larger than that for the disordered sample and that of the latter saturates at slightly lower fields. This is consistent with a more collective behavior in the supracrystal compared to the disordered sample. It is reasonable to imagine that the flipping of the spins could require higher fields when the nanocrystals are ordered in a long-range superlattice compared to the disordered system, where we have only very short-range order. The first magnetic intrinsic property as a result of the ordering is observed.[39,40]

The magnetic properties also markedly differ with the shape of the arrangement of nanocrystals in the mesoscopic structure. This is demonstrated by using 10 nm γ-Fe_2O_3 nanocrystals, differing by the number of carbon atoms forming the surfactant used to coat them (see above). As shown above, nanocrystals are able to assemble to form long wires (Figure 7a) or a film (Figure 7b) when the number of carbon atoms of the surfactant increases from 8 to 12. When the applied field direction is along the long axis (*x* direction) of the wire, the reduced remanance increases compared to that obtained when the applied field is along the short axis (*y* direction). Conversely, no change in the magnetization curves, with the direction of the applied field, are observed when the 10 nm γ-Fe_2O_3 nanocrystals are coated with C12 carbon atoms and form a homogeneous film (Figure 7c). From an energetic viewpoint, we could explain this by the orientation of the easy axes of nanocrystals when they are subjected to an applied field. In such a case, this has to be confirmed by Mossbauer spectroscopy. For a total orientation of the easy axes, the relative intensities of the Mossbauer spectra are expected, for γ-Fe_2O_3 nanocrystals, to be 1,4,3, whereas for a total disorder, the Mossbauer spectra are expected to be 1,2,3. Experimentally, for disordered aggregates (Figure 7d) and the film (Figure 7f), the Mossbauer relative peaks intensity is, as expected, 1,2,3, whereas for wires, it is 1, 2.14, and 3 (Figure 7e). Such a slight change in the relative Mossbauer intensity (from 2 to 2.14) indicates that very few nanocrystals have their easy axis oriented. The hysteresis loop, calculated with a 2.14 relative peak intensity, shows no change compared to that obtained for 2.[26] Therefore, a slight change in the relative Mossbauer intensity indicates that very few nanocrystals have their easy axis oriented. From the change in the magnetic properties of the assembly-forming wires (Figure 7a) compared to films (Figure 7b), both made with the same batch of nanocrystals, it can be claimed that the change is due to the shape of the mesoscopic structure.[42] Note that a similar magnetic behavior is observed when the easy axes of the nanoc-

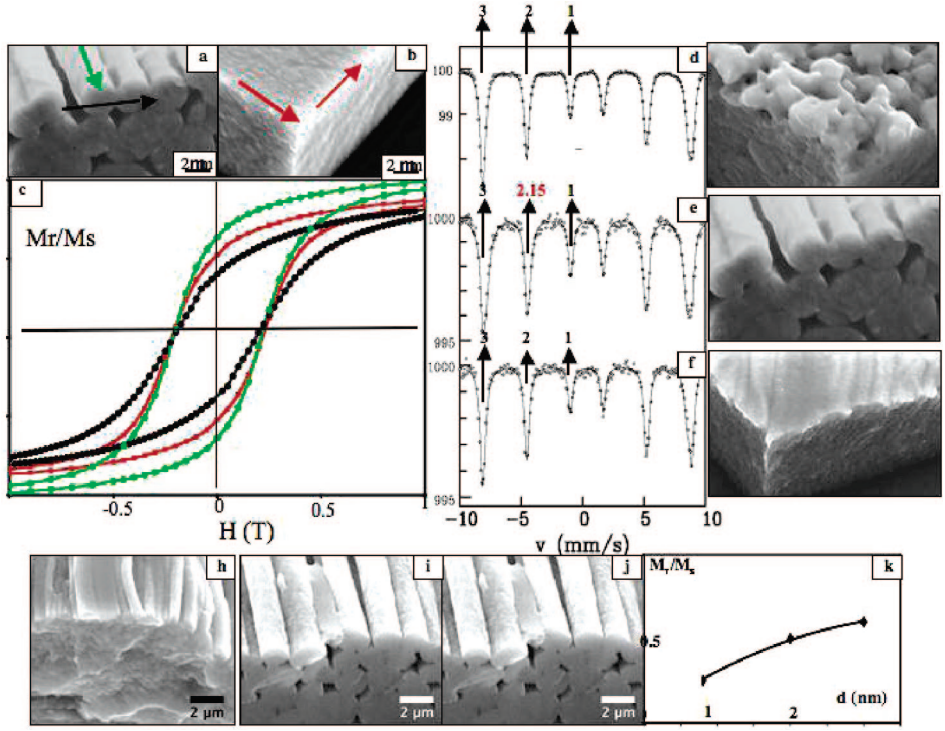

FIGURE 7. SEM images of shaped γ-Fe_2O_3 nanocrystals coated with either (a) citrate ions and forming tubes or (b) decanoic acid and forming a thin film with undulations. Magnetization curves at 3 K of tubes recorded either parallel with (green), perpendicular to (black), or on the film under (red) the two directions.

rystals are oriented but the explanation differs.[43] This means that wires of nanocrystals behave as bulk ones. This would be confirmed if the reduced remanance of the our wires decreases with their widths, as with bulk wires. Figure 7k shows an increase in the reduced remanance with the size of their widths, produced by changing the strength of the applied field used during the deposition (parts h–j of Figure 7). Here, the shape of the mesoscopic structure controls the change in the magnetic properties.

4. Epitaxial Crystal Growth as a Result of the Nanocrystal Ordering. In the following, we use 5 nm silver nanocrystals similar to those described above. The major differences are that the nanocrysals are coated with decanethiol instead of dodecanethiol and dispersed in decane instead of hexane. Two types of TEM grids are used: one is covered by amorphous carbon, and the other HOPG is stuck on the grid. In each experiment, two similar TEM grids are immersed in a beaker containing the solution and kept in an oven at 50 °C. One grid is extracted from the oven after decane evaporation (20 h), whereas the second remains in the oven for 8 days. At the end of each process, the TEM grid is kept at room temperature. Whatever the substrate is, mono- (2D) and multi- (3D) layers of nanocrystals are formed. However, some marked differences are observed: on amorphous carbon, multilayer nanocrystal assemblies (3D) are not well-organized (Figure 8a) as confirmed by power spectra (PS), with one ring and diffuse spots at the first order (Figure 8b) indicating organization of nanocrystals in small domains. After 8 days of annealing, the TEM image shows the formation of particles having various shapes (Figure 8c). Many of the particles are multiply-twinned particles (MTPs; inset of Figure 8c), with the presence of a small amount of flat triangles (see red arrows in Figure 8c) with rounded edges. The TEM image of the flat triangular particle in a bright field (Figure 8d) shows an uniform contrast, whereas very bright faceted particles are obtained by a dark field image (Figure 8f). This indicates a strongly diffracting crystal and, consequently, a well-crystallized object. This is confirmed by high-resolution (HR)TEM patterns with a fcc structure and a very high crystallinity. Here, the formation of triangular flat fcc single crystals is observed.

When amorphous carbon is replaced with HOPG, the nanocrystals are highly ordered in 2D and 3D. TEM images obtained at the end of the evaporation show long-distance organization (Figure 8f). This is confirmed with a PS (Figure 8g) characterized by several well-defined sharp spots at the first and second order, indicating an ordering over large domains. In TEM patterns, observed after annealing the sample at 50 °C for 8 days, very large triangular-shape crystals appear that are equilateral, flat, and more or less truncated at the edges (Figure 8h). Several triangular particles seem to be aligned on the substrate (see red lines on Figure 8h). Because the experiments are done under the same experimental conditions as those described above, these preferential orientations are induced by the HOPG substrate. The average size is 9 times larger (940 nm) than those obtained on amorphous carbon. A few decahedral particles with maximum sizes $\leq$200 nm with pentagonal or rhombic profiles are also produced (see particles surrounded by

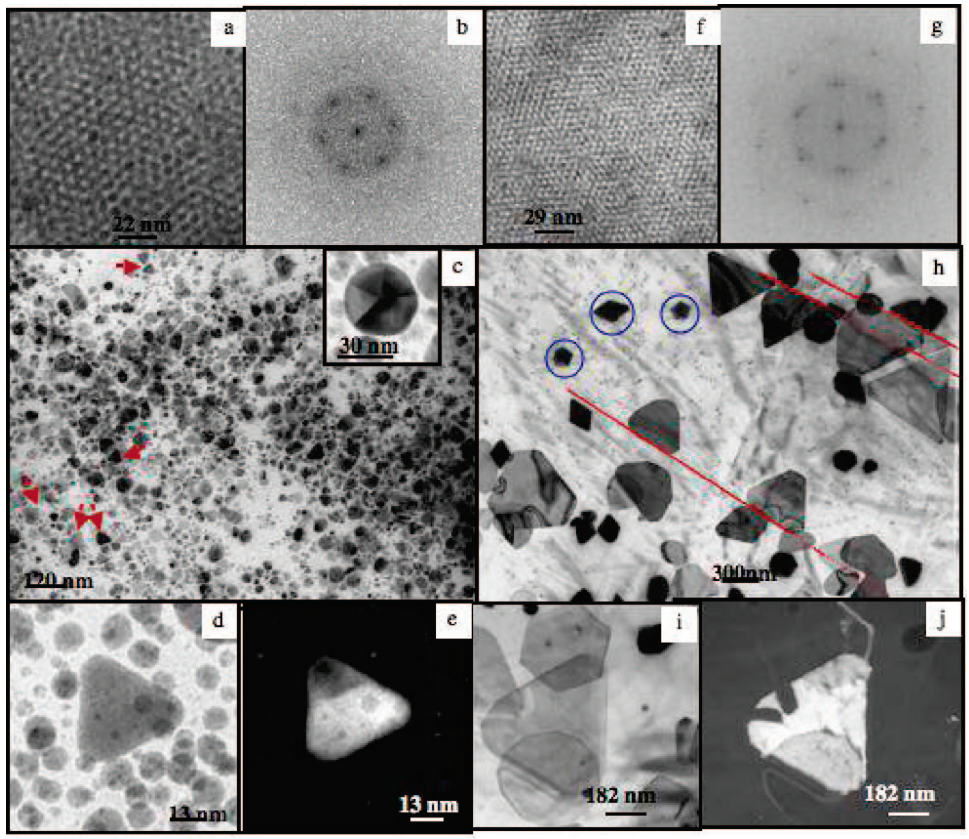

FIGURE 8. Three-dimensional silver nanocrystal organization and corresponding PS deposited on amorphous carbon (a and b) and HOPG (f and g). TEM patterns and bright and dark fields observed after annealing the samples during 8 days with amorphous carbon (c–e) and HOPG (h–j) as substrates.

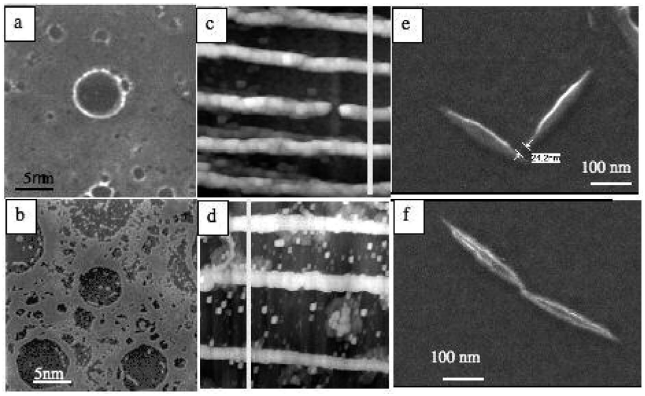

FIGURE 9. Atomic force microscopy (AFM) patterns of γ-Fe_2O_3 nanocrystals self-organized in rings and lines before (a and b) and after (c and d) etching, respectively. Field emission gun (FEG)–SEM patterns of transferred needles after etching ($O_2 + SF_6$) with different spacings: 24.2 nm (c) and 0 nm (d).

circles in Figure 8h). The HRTEM measurements of these particles show that the crystallinity of the particles is very high, even at the edges. The formation of thin single crystals is confirmed by TEM images in bright (Figure 8i) and dark (Figure 8j) fields. An epitaxial growth on HOPG of triangular single-crystals is demonstrated by TEM diffractions performed on several isolated triangular particles.[44] With amorphous carbon and HOPG as substrate, single crystals are formed. However, their sizes differ. This is related to the long-range ordering of the silver nanocrystals. Coalescence of some native nanocrystals to triangular single crystals characterized by a three-fold symmetry is due to the progressive removal of the alkyl chains by light annealing (50 °C), with the appearance of coalescence followed by a surface reconstruction to form single crystals. This process is favored by the small nanocrystal interdistance (≠2 nm) and by the dimensions of the ordered nanocrystal domains. The mechanism of epithaxial growth on HOPG seems similar to that observed by bulk silver evaporation under ultra high vacuum (UHV) at high temperatures (≥300 °C).[45–47] However, the sizes are much smaller than those obtained on HOPG.[44] Here, the domain size of ordered nanocrystals controls that of triangular single crystals. A hepitaxial growth is observed when the substrate is a crystal as HOPG.

5. Colloidal Lithographic Growth. Nanotechnology research is led by the demand for ever smaller device features needed to improve performance and decrease costs in microelectronics, communication, and data storage. Various lithographic methods have been developed in the last few years and are in the center of this nanotechnology. Very few methods provide the ability to work in the sub-50 nm scale. One of the possibilities is to use nanocrystals as masks, and we impose a pattern on the SiO_2 substrate. To do this, we first need to clean it and deposit polymethylmethacrylate (PMMA). γ-Fe_2O_3 nanocrystals (10 nm) are then deposited, forming rings[7] (Figure 9a) or lines (Figure 9b), and the pattern transfer onto the material is performed by reactive ion etching

(RIE). As shown in parts b and c of Figure 9, respectively, the rings and lines are still observed, proving that 10 nm γ-Fe_20_3 nanocrystals can be used as lithographic masks.[48] This was seen at the micrometer scale, and we need to be able to discern a few nanometers. Using cigar-like-shape γ-Fe_20_3 particles with 320 nm length and an aspect ratio of 7, their shapes are retained when the distance between particles is around 10 nm (parts b and c of Figure 9).[49] With this technique, it is possible to use γ-Fe_20_3 nanocrystals as masks for lithography.

Special thanks are due to my colleagues Drs. A. Courty, N. Goubet, D. Ingert, I. Lisiecki, T. Ngo, D. Parker, C. Petit, and J. Richardi.

References

(1) Sanders, J. V. Color of precious opal. *Nature* **1964**, *204*, 1151–1153.
(2) Bazylinski, D. A.; Frankel, R. B. Magnetosome formation in prokaryotes. *Nat. Rev. Microbiol.* **2004**, *2*, 217–230.
(3) Lopez, C. Materials aspects of photonic crystals. *Adv. Mater.* **2003**, *15*, 1679–1704.
(4) Warren, S. C.; Disalvo, F. J.; Wesner, U. Nanoparticles—Tuned assembly and disassembly of mesostructured silica hybrids. *Nat. Mater.* **2007**, *6*, 154–161.
(5) Motte, L.; Billoudet, F.; Pileni, M.-P. Self-assembled monolayer of nanosized particles differing by their sizes. *J. Phys. Chem.* **1995**, *99*, 16425–16429.
(6) Murray, C. B.; Kagan, C. R.; Bawendi, M. G. Self-organization of CdSe nanocrystallites into three-dimensional quantum dot superlattices. *Science* **1995**, *270*, 1335–1338.
(7) Pileni, M.-P. Organization in 2D and 3D superlattices. *J. Phys. Chem. B* **2001**, *105*, 3358–3371.
(8) Pileni, M.-P. Self-organization of inorganic nanocrystals. *J. Phys.: Condens. Matter* **2006**, *18*, S65–S84.
(9) Brust, M.; Bethell, D.; Schiffrin, D. J.; Kiely, C. Novel gold-dithiol nano-networks with non-metallic electronic properties. *Adv. Mater.* **1995**, *9*, 795–797.
(10) Harfenist, S. A.; Wang, Z. L.; Alvarez, M. M.; Vezmar, I.; Whetten, R. L. Highly oriented molecular Ag nanocrystal arrays. *J. Phys. Chem.* **1996**, *100*, 13904–13910.
(11) Motte, L.; Billoudet, F.; Lacaze, E.; Pileni, M.-P. Self organization of nanosized particles differing by their size into three dimensional superlattices. *Adv. Mater.* **1996**, *8*, 1018–1020.
(12) Whetten, R. L.; Khoury, J. T.; Alvarez, M. M.; Murthy, S.; Vezmar, I.; Wang, Z. L.; Stephens, P. W.; Cleveland, C. L.; Luedtke, W. D.; Landman, U. Nanocrystal gold molecules. *Adv. Mater.* **1996**, 428–433.
(13) Murthy, S.; Wang, Z. L.; Whetten, R. L. Thin films of thio-derivatized gold nanocrystals. *Philos. Mag. Lett.* **1997**, *75*, 321–327.
(14) Korgel, B. A.; Fitzmaurice, D. Small-angle X-ray-scattering study of silver-nanocrystal disorder–order phase transitions. *Phys. Rev. B: Solid State* **1999**, *59*, 14191–14201.
(15) Zeng, H.; Sun, S.; Sandstrom, R. L.; Murray, C. B. Chemical ordering of FePt nanoparticle self-assemblies by rapid thermal annealing. *J. Magn. Magn. Mater.* **2003**, *266*, 227–232.
(16) Yang, H. T.; Shen, C. M.; Su, Y. K.; Yang, T. Z.; Gao, H. J. Self-assembly and magnetic properties of cobalt nanoparticles. *Appl. Phys. Lett.* **2003**, *82*, 4729–4731.
(17) Courty, A.; Fermon, C.; Pileni, M.-P. Supra crystals made of metal silver nanocrystals. *Adv. Mater.* **2001**, *13*, 254–258.
(18) Courty, A.; Araspin, O.; Fermon, C.; Pileni, M.-P. Supra crystals made of nanocrystals: Growth on HOPG substrate. *Langmuir* **2001**, *17*, 1372–1380.
(19) Courty, A.; Mermet, A.; Albouy, P. A.; Duval, E.; Pileni, M.-P. Self-organized Ag-nanocrystals in fcc "supra" crystals: Vibrational coherence. *Nat. Mater.* **2005**, *4*, 395–400.
(20) Zaitseva, N.; Rong Dai, Z.; Leon, F. R.; Krol, D. Optical properties of CdSe superlattices. *J. Am. Chem. Soc.* **2005**, *127*, 10221–10226.
(21) Lisiecki, I.; Albouy, P. A.; Pileni, M.-P."Supra crystals" made of cobalt nanocrystals. *Adv. Mater.* **2003**, *15*, 712–716.
(22) Lisiecki, I.; Albouy, P. A.; Pileni, M.-P. Supra-crystal: Control of the ordering of cobalt nanocrystals self-assemblied at the mesoscopic scale. *J. Phys. Chem. B* **2004**, *108*, 20050–20055.
(23) Zeng, N.; Fan, J.; Stucky, G. D. One-step one phase synthesis of monodisperse nobel-metallic nanoparticles and their colloidal crystals. *J. Am. Chem. Soc.* **2006**, *128*, 6550–6551.
(24) Taleb, A.; Petit, C; Pileni, M.-P. Optical properties of self-assembled 2D and 3D superlattices of silver nanoparticles. *J. Phys. Chem.* **1998**, *102*, 2214–2220.
(25) Petit, C.; Taleb, A.; Pileni, M.-P. Self-assembled in 2D of cobalt nanosized particles. *Adv. Mater.* **1998**, *10*, 259–261.
(26) Russier, V.; Petit, C.; Pileni, M.-P. Hysteresis curve of magnetic nanocrystals monolayers: Influence of the structure. *J. Appl. Phys.* **2003**, *93*, 10001–10010.
(27) Pileni, M.-P. Reverse micelles: A microreactor. *J. Phys. Chem.* **1993**, *97*, 6961–6973.
(28) Motte, L.; Lacaze, E.; Maillard, M.; Pileni, M.-P. Self-assemblies of silver sulfide nanocrystals on various substrates. *Langmuir* **2000**, *16*, 3803–3812.
(29) Lalatonne, Y.; Richardi, J.; Pileni, M.-P. Van der Waals versus dipolar forces controling mesoscopic organizations of magnetic nanocrystals. *Nat. Mater.* **2004**, *3*, 121–126.
(30) Germain, V.; Pileni, M.-P. Dots and labyrinthines of cobalt nanocrystals. *Adv. Mat.* **2005**, *17*, 1424–1230.
(31) Germain, V.; Pileni, M.-P. Mesostructures of cobalt nanocrystals: Mechanism. *J. Phys. Chem* **2005**, *109*, 5548–5553.
(32) Germain, V.; Richardi, J.; Ingert, D.; Pileni, M.-P. Mesostructures of cobalt nanocrystals: Experiment and theory. *J. Phys. Chem. B* **2005**, *109*, 5541–5547.
(33) Palpant, B.; Portales, H.; Saviot, L.; Lermé, J.; Prével, B.; Pellarin, M.; Duval, E.; Perez, A.; Broyer, M. Quadrupolar vibrational mode of silver clusters from plasmon-assisted Raman scattering. *Phys. Rev. B: Solid State* **1999**, *60*, 17107–17111.
(34) Duval, E.; Boukenter, A.; Champagnon, B. Vibration eigenmodes and size of microcrystallites in glass: Observation by very low frequency Raman scattering. *Phys. Rev. Lett.* **1986**, *56*, 2052–2055.
(35) Portales, H.; Saviot, L.; Duval, E.; Fujii, M.; Hayashi, S.; Del Fatti, N.; Vallée, F. Resonant Raman scattering by breathing modes of metal nanoparticles. *J. Chem. Phys.* **2001**, *115*, 3444–3447.
(36) Duval, E.; Mermet, A.; Courty, A.; Albouy, P. A.; Pileni, M.-P. Raman scattering from self-organized Ag-nanocrystals in "supra" crystals: Theory. *Phys. Rev. B: Solid State* **2005**, *72*, 85439–85444.
(37) Bigot, J. Y.; Lisiecki, I.; Halte, V.; Petit, C.; Pileni, M.-P. Femtosecond dynamic of cobalt supra crystals. Unpublished data.
(38) Taleb, A.; Silly, F.; Gussev, A. O.; Charra, F.; Pileni, M.-P. Electron transport properties of nanocrystals: Isolated or in "supra" crystalline phases. *Adv. Mater.* **2000**, *12*, 633–637.
(39) Lisiecki, I.; Parker, D.; Salzemann, C.; Pileni, M.-P. An intrinsic magnetic property due to the mesoscopic ordering of cobalt nanocrystals in supra-crystals. Manuscript submitted for publication to *Chem. Mat.*
(40) Parker, D.; Lisiecki, I.; Salzemann, C.; Pileni, M.-P. Emergence of new collective properties of cobalt nanocrystals ordered in fcc supra-crystals: Magnetic investigation. Manuscript submitted for publication.
(41) Dormann, J. L.; Spinu, L.; Tronc, E.; Jolivet, J. P.; Lucari, F.; D'orazio, F.; Fiorani, D. Effect of interparticle interactions on the dynamical properties of γ-Fe_2O_3 nanoparticles. *J. Magn. Magn. Mater.* **1998**, *183*, L255–L260.
(42) Lalatonne, Y.; Motte, L.; Russier, V.; Ngo, A. T.; Bonville, P.; Pileni, M.-P. Mesoscopic structures of maghemite nanocrystals: Collective magnetic properties due to the alignment of nanocrystals. *J. Phys. Chem. B* **2004**, *108*, 1848–1854.
(43) Ngo, A. T.; Pileni, M.-P. Cigar-shaped ferrite nanocrystals: Orientation of the easy magnetic axes. *J. Appl. Phys.* **2002**, *92*, 4649–4652.
(44) Courty, A.; Henry, A. I.; Goubet, N.; Pileni, M.-P. Growth of large triangular silver single crystals from 5 nm self-organized silver nanocrystals: Epitaxial growth on HOPG at 50 °C. Manuscript submitted for publication to *Nature Materials*.
(45) Yagi, K.; Takayanagi, K.; Kobayashi, K.; Honjo, G. In-situ observations of growth processes of multiply twinned particles. *J. Cryst. Growth* **1975**, *28*, 117–124.
(46) Doraiswamy, N.; Jayaram, G.; Marks, L. D. Unusual island structures in Ag growth on Si(100)-(2 × 1). *Phys. Rev. B: Solid State* **1995**, *51*, 10167–10170.
(47) Chapon, C.; Granjeaud, S.; Humbert, A.; Henry, C. R. Structure and morphology of nanometer-sized Pd clusters grown at high temperature on natural graphite single crystals. *Eur. Phys. J.: Appl. Phys.* **2001**, *13*, 23–30.
(48) Ingert, D.; Pileni, M.-P. Nanocrystals used as mask, nanolithography. *J. Phys. Chem. B* **2003**, *107*, 9617–9619.
(49) Ingert, D.; Pileni, M.-P. Colloidal nano litography. Manuscript to be submitted for publication.

AR6000582